

Phase closure nulling of HD 59717 with AMBER/VLTI[★]

Detection of the close faint companion

G. Duvert, A. Chelli, F. Malbet and P. Kern

Laboratoire d’Astrophysique de Grenoble and Mariotti Center, UMR 5571 Université Joseph Fourier/CNRS, B.P. 53, 38041 Grenoble Cedex 9, France
e-mail: Gilles.Duvert@obs.ujf-grenoble.fr

date received; date accepted

ABSTRACT

Aims. The detection of close and faint companions is an essential step in many astrophysical fields, including the search for planetary companions. A new method called “phase closure nulling” has been proposed for the detection of such faint and close companions based on interferometric observations when the system visibility amplitude is close to zero due to the large diameter of the primary star. We aim at demonstrating this method by analyzing observations obtained on the spectroscopic binary HD 59717.

Methods. Using the AMBER/VLTI instrument in the K-band with ~ 1500 spectral resolution, we record the spectrally dispersed closure phases of the SB1 binary HD 59717 with a three-baseline combination adequate for applying phase closure methods. After a careful data reduction, we fit the primary diameter, the binary flux ratio, and the separation using the phase closure data.

Results. We detect the 5-mag fainter companion of HD 59717 at a distance of 4 stellar radii from the primary. We determine the diameter of the primary, infer the secondary’s spectral type and determine the masses and sizes of the stars in the binary system. This is one of the highest contrasts detected by interferometry between a companion and its parent star.

Key words. stars: fundamental parameters – stars: individual: HD 5917 – binaries: close – binaries: spectroscopic – techniques: interferometric – astrometry

1. Introduction

Since the first firm discoveries of planetary-mass companions to stars, there has been a renewed interest in all the observational techniques that can provide reliable estimates of binary masses and distances. Beside the mass, the most desirable information and the most difficult to measure is the spectrum of the companion. Imaging the close environment of stars is a very active research field (Marois et al. 2008; Kalas et al. 2008; Lagrange et al. 2009), and is the main motivation for several ambitious instruments proposed recently (Cockell et al. 2009; Lawson et al. 2008), based either on fringe nulling (Bracewell 1978; Woolf & Angel 1998) or “extreme” adaptive optics and coronagraphy (see review by Beuzit et al. 2007). These techniques are complementary to interferometric imaging since they are blind to regions within a few Airy disks from the central star, whereas the interferometric observables acquired by spatially-filtered interferometers largely come from within this Airy disk.

A large fraction of the observational effort of current optical long-baseline interferometers is devoted to the study of the close environment of stars. By using spatial filtering techniques, the interferometers have gained in precision and stability. Using more than two apertures simultaneously, together with a large spectral coverage, near infrared beam combiner like the AMBER/VLTI instrument (Petrov et al. 2007), can provide precise measurements of these close environments, of less than a few hundred stellar radii. We have recently proposed a new inter-

ferometric technique called “phase closure nulling¹” (hereafter PCN), to detect and to perform the spectroscopy of faint companions of stars (Chelli et al. 2009a). This technique is based on the modeling of spectrally dispersed phase closure measurements of the multiple system around visibility zeros of the primary. In these regions, there is always a spatial frequency interval within which the phase closure signature of the companion is *larger than any systematic error* and is thus *measurable*.

We illustrate the proof of concept of PCN with a simple observational case, the bright single-lined spectroscopic binary HD 59717. Although the observations were not initially intended for this purpose, and are thus very incomplete, we can nevertheless derive the characteristics of the system in terms of stellar diameter, separation and flux ratio. The observations and the data reduction are presented in Sect. 2. Section 3 describes the derivation of the binary parameters, from visibility and phase closure measurements. The results are discussed in Sect. 4.

2. Observations and data reduction

2.1. Observations

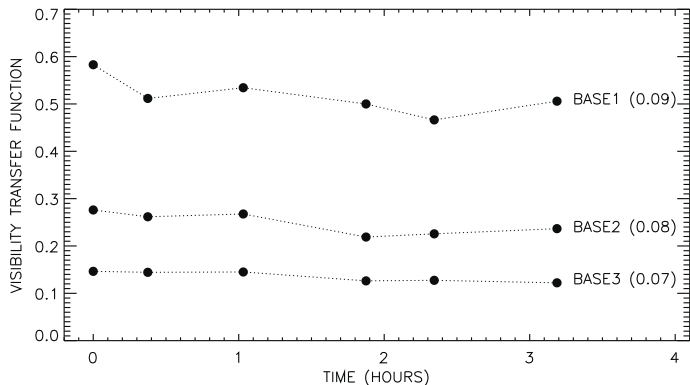
The observations are part of a series of on-sky tests performed to assess the stability of the AMBER instrument and the corresponding accuracy of absolute calibration. They were performed after a change of the infrared detector and the temporary removal, by our team, of a set of polarisers that was inducing

[★] Based on observations collected at the European Southern Observatory, Paranal, Chile, within the commissioning programme 60.A-9054(A).

¹ Not to be confused with the “Three-Telescope Closure-Phase Nulling Interferometer Concept” proposed by Danchi et al. (2006) which deals with the phase closure properties of *nulling interferometers*.

Table 1. Summary of observation log. Uniform disk diameters for calibrators were obtained with the use of SearchCal (Bonneau et al. 2006).

Name	Date	Time of observation (UTC)	Sp. Type	Mag. K	θ_{UD} (mas)	Fringe tracker	Spectral coverage (nm)	DIT (ms)
HD 59717	2008-02-13	03:03:07, 05:40:59	K5III	-0.41	-	yes	[1925-2275]	200
HD 56478	2008-02-13	02:26:23, 04:26:38	K0III	4.48	0.618 ± 0.043	yes	[1925-2275]	200
HD 37350	2008-02-13	05:04:59	F6Ia	2.09	0.643 ± 0.026	yes	[1925-2275]	200
HD 59717	2008-02-14	03:02:50, 04:51:56, 06:11:50	K5III	-0.41	-	no	[2110-2190]	50
HD 70555	2008-02-14	03:27:16, 05:18:42, 06:40:03	K1III	1.53	2.54 ± 0.037	no	[2110-2190]	50
HD 45669	2008-02-14	03:49:44, 04:26:21, 05:48:39	K5III	1.88	2.19 ± 0.053	no	[2110-2190]	50

**Fig. 1.** Transfer function computed from the 6 calibrator observations carried out on 14 February 2008 as a function of time for the 3 baselines (shortest baseline at the top). The numbers in parenthesis are the relative visibility dispersion.

Fabry-Pérot fringe beating, leading to instabilities in the instrumental visibility (Malbet et al. 2008). As a consequence of this removal, the fringe contrast decreased, but the stability improved drastically. To characterize the stability, we observed a series of calibrator stars of various magnitudes, at different locations in the sky, taken from the ESO list of VLTI calibrators. One of these stars, HD 59717, is a triple system located at 56.3 pc, consisting of a K5III single-lined spectroscopic binary and a G5V companion at $22''.3$ distance (MSC catalog, Tokovinin 1997). The companion was not in the field of view of the AMBER observations, and we will refer hereafter to the SB1 close binary as HD 59717.

We used three 1.8m auxiliary telescopes (ATs) on VLTI stations H0, D0 and A0. In this configuration, the 3 telescopes are aligned in a very rough East-West (71°) configuration and the ground baseline lengths are A0-D0: 32 m, D0-H0: 64 m, A0-H0: 96 m. Due to its large angular size, HD 59717 is well resolved in the H0-D0-A0 configuration, the longest baseline crossing by supersynthesis effect the first zero of the visibility curve and providing information in the first and the second lobes.

Our set of data consists of three observations of HD 59717 performed on 14 February 2008, using the spectral window 2110–2190nm and a detector integration time (DIT) of 50 ms. Each observation was bracketed with those of the calibrators HD 70555 and HD 45669. Additionally, we make use of a single visibility measurement taken from an observation performed the previous night with FINITO, the VLTI fringe tracking facility (Gai et al. 2004). This observation covers the wavelength range 1925–2275 nm, used a DIT of 200 ms, and was bracketed with observations of the calibrators HD 56478 and HD 37350.

2.2. Data reduction

Prior to the data reduction, we performed an accurate wavelength calibration thanks to the identification of atmospheric features in the spectrum obtained from the single observation with FINITO. We fit the position of the atmospheric features with a second degree polynomial, providing a precision of a few nanometers. Then, the data were reduced with the new AMBER data reduction method presented in Chelli et al. (2009b).

Figure 1 shows the instrumental transfer function averaged in wavelength, obtained for the 3 baselines as a function of time. This transfer function results from the ratio of the measured visibility and the intrinsic visibility of the calibrator. The number between parenthesis is the relative visibility dispersion, computed for each baseline, as the ratio between the dispersion of the visibilities along the night and their mean. This is the dominant source error due to a residual atmospheric jitter during the frame integration time. Other sources of error are negligible in this respect. The intrinsic visibilities have been derived from diameters estimated with the SearchCal software (Bonneau et al. 2006) and their associated relative error is much smaller, less than 0.8% for the largest calibrator on 100m baseline. The high spectral resolution (1500) prevents any spectral mismatch between source and calibrators. Except for the single visibility data in the second lobe obtained with FINITO (see below), the two magnitude difference between the source and the calibrators does not matter as, in the absence of a fringe-tracking system, the jitter is flux-independent. In the spectral range 2110–2190 nm, the transfer function is a linear function of the wavelength. We use this *a priori* information to reduce the high frequency noise on the calibrator visibilities by Fourier filtering.

The visibility data of HD 59717 obtained with the assistance of the fringe tracker (see Table 1) are affected by a residual, flux-dependent, jitter that will be different on our source and its calibrators due to their magnitude difference. In principle, we can apply a jitter correction to the data. Unfortunately, the jitter residuals from the fringe tracking system were not included at the time in the instrumental data. Only one visibility of high quality, measured in the second lobe, could be calibrated with the aid of partially redundant visibilities obtained during the second night.

The peculiarity of AMBER is to use an internal calibration called P2VM to estimate the coherent fluxes. Hence, the phase closure on a source contains the imprints of the P2VM. Since, during the building process, the three beams are measured independently, the internal phase closure of the P2VM is not by construction constrained to be zero. This is why a phase closure measurement with AMBER must be calibrated by subtracting that of a calibrator. The three (spectrally dispersed) phase clo-

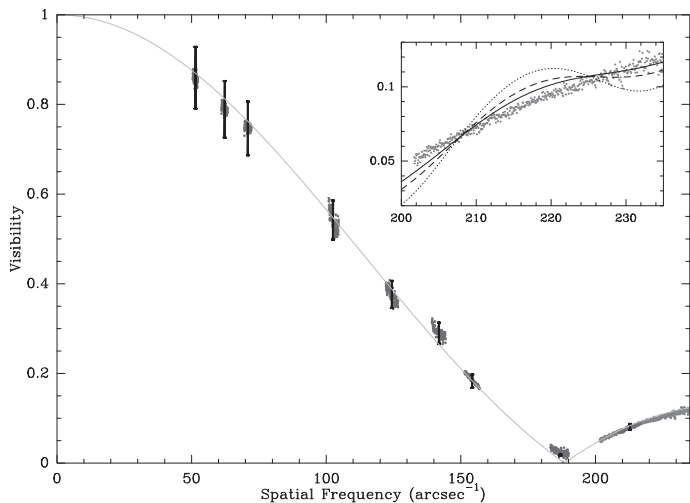


Fig. 2. Visibility of HD 59717 as a function of the spatial frequency. Errorbars illustrate the calibration errors resulting from the visibility dispersion shown in Fig. 1. The measurements obtained with the fringe tracker are plotted in grey in the second lobe. The full curve corresponds to a single uniform disk model of diameter 6.436 mas. The insert shows the second lobe measurements and three binary models with separation 30 mas and flux ratio: 5×10^{-3} (continuous line), 1×10^{-2} (dashed line), 2×10^{-2} (dotted line).

ures measured just before, during and after the minimum of visibility have been corrected by the phase closure of a calibrator star close in time. The main error, due to the calibration process, is about 0.05 radian from the internal dispersion of the calibrator phase closure measurements along the night. To reduce the phase closure dispersion, especially at minimum visibility, we average the bispectra (from which the phase closure is computed), initially sampled with a frequency interval of 0.06 arcsec^{-1} , within a frequency interval of 1 arcsec^{-1} .

3. Results

The calibrated visibilities of HD 59717 are shown in Fig. 2 as a function of the spatial frequency, defined as the ratio between the baseline and the wavelength. The measurements are reasonably uniformly spread over the working frequency range, with a set of measurements before, partially during, and after the minimum visibility. The full curve represents the best fit (excluding the points around minimum of visibility, see Sect. 3.1) with a single uniform disk model of diameter 6.436 mas. This is in excellent agreement with the diameter of $6.44 \pm 0.06 \text{ mas}$ arising from the location of the minimum of visibility around $189 \pm 0.02 \text{ arcsec}^{-1}$.

The phase closures are shown in Fig. 3. The transition between the 0 and π values at the zero visibility crossing is smooth, markedly different from the expected abrupt step arising from a centrally symmetric flux distribution only (see Chelli et al. 2009a).

This departure from a centrally-symmetric object is expected in a spectroscopic binary, and we can use these observations to retrieve the geometric characteristics of the system. To do this, we fit independently the visibility and the closure phase data with a simple model formed by an extended uniform disk and a point source. We did not try to combine visibility and closure phase data because the weight to give to each set of data is quite

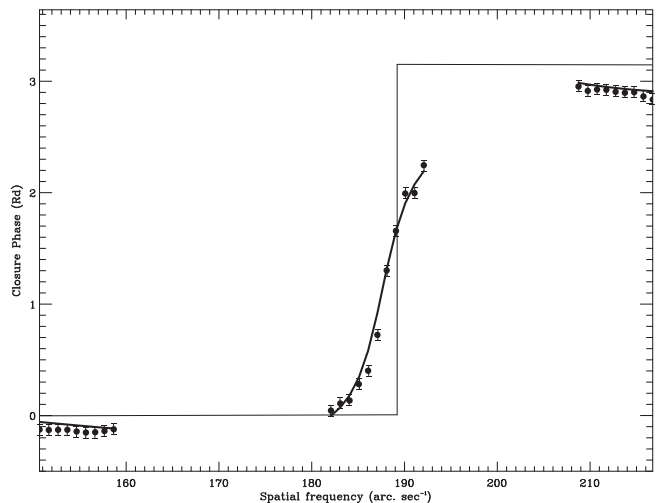


Fig. 3. Phase closure of HD 59717 as a function of the largest spatial frequency of the closure triangle. The thin curve corresponds to the best fit for a single uniform disk model with diameter 6.451 mas. The full curve corresponds to the best fit with a double system and parameters: primary stellar diameter 6.55 mas, secondary projected distance -11.2 mas and flux ratio 0.017.

uncertain. Our observations being basically east-west, we cannot derive the position angle of the system, but only the projected distance along the direction of observation. As we have used the spectral dimension to increase the frequency coverage, we assume that the object is achromatic. Hence our model is described by 3 parameters: the stellar diameter, the distance of the companion and the flux ratio.

3.1. Visibility data

To estimate the system parameters, we minimize a standard χ^2 defined as the distance between the visibilities of the model and those of the data, weighted by the errors shown in Fig. 1. We exclude from the fit the set of points around minimum visibility as they may easily be biased. Indeed, at this location, the bias on the squared amplitude of the coherent flux is twenty times larger than the useful (debiased) signal. Given the relative error of 0.07 on our longest baseline, an imprecision of $0.07/\sqrt{20} = 1.5 \cdot 10^{-2}$ would produce a bias “error” equivalent to the statistical error. Since we are not guaranteed such a precision in the bias removal, it is better to exclude this set of points, which otherwise would constrain nearly by itself the output of the fit. This restriction does not apply if a single stellar diameter is deduced from the *position* of the minima of visibility, since the location of the minima are much less biased.

A rapid study of the problem shows that the χ^2 has minima as a function of the distance with a pseudo-period $p \approx f_{min}^{-1}$, where f_{min}^{-1} is the frequency of minimum visibility. Hence to produce comprehensible output, we vary the separation from 0 to 0.1 arcsec, and for each separation, we perform a fit with two parameters, the stellar diameter and the flux ratio. The minimum reduced χ^2 (hereafter χ^2), the best stellar diameters and flux ratio are displayed in Fig. 4 as a function of the separation.

The χ^2 presents shallow minima between 1.3 (single source) and 0.9 (double source) at a set of roughly regularly separations. However, given that below 1% precision, the calibration biases on the visibility become dominant, the presence of these minima

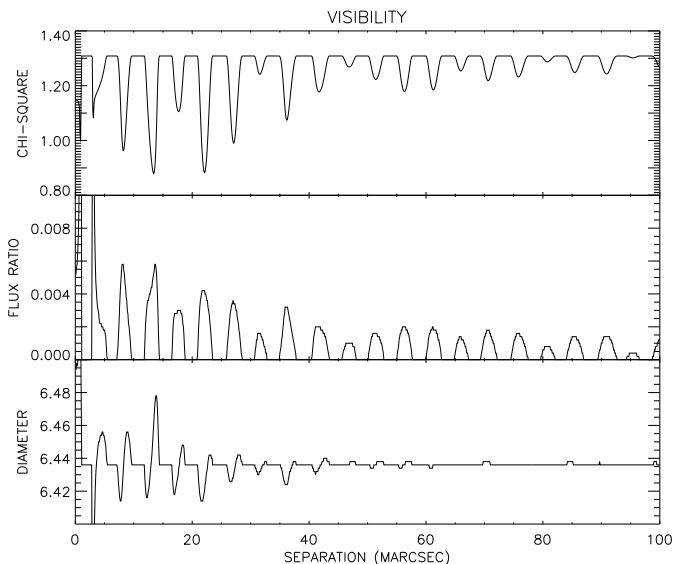


Fig. 4. Best model parameters from visibility fit with an extended uniform disk and a point source (see Sect. 3.1 for details). From top to bottom as a function of the separation: minimum χ^2 , best flux ratio and best stellar diameter.

alone does not prove the binary nature of HD 59717. In addition, their location must be taken with extreme caution. If we except the singular point around 3 mas inside the stellar disc, the range of possible stellar diameters for all the separations is 6.45 ± 0.03 mas. This diameter range agrees with the output of the fit with a single uniform disk model of 6.436 mas (see Fig. 2). The possible flux ratio ranges from 10^{-3} to 6×10^{-3} for all separations and, the smaller the separation the higher the flux ratio.

3.2. Phase closure data

The best fit of the phase closure systems with a single uniform disk model provides a diameter of 6.451 mas in excellent agreement with the value of 6.436 mas derived from visibility data. The minimum χ^2 of a two-component model, the best stellar diameters and flux ratio are displayed in Fig. 5 as a function of the separation. This minimum χ^2 varies from 120 (single source) to 2.3 (double source).

The stellar diameter ranges between 6.2 and 6.7 mas. It is not well constrained because we do not have the full transition, but only pieces of it. The flux ratio varies between 6×10^{-3} and 2.7×10^{-2} , which corresponds to a $5^{+0.55}_{-0.75}$ mag difference between the primary and the secondary. The slope of the phase closure is extremely sensitive on the flux ratio. To illustrate this effect, we plotted in Fig. 6 the phase closure together with the best fit for various flux ratios. One sees that all flux ratios $\leq 5 \times 10^{-3}$ cannot reproduce the slope of the transition.

The χ^2 (Fig. 5) exhibits regularly spaced and very deep minima as a function of the separation. The minimum flux ratio of 5×10^{-3} obtained in the fits renders separations larger than 30 mas irrelevant, as they would produce oscillations that are not seen in the visibility, especially in the second lobe (see insert in Fig. 2). Hence, the possible projected separations left are -5.5 , $+8.5$, -11 , $+14$ and -17 mas, with an error of ~ 1 mas, from the width at mid-height of the χ^2 dips.

In summary, visibility data put strong constraints on the stellar diameter, 6.45 ± 0.03 mas. Phase closure data do not constrain

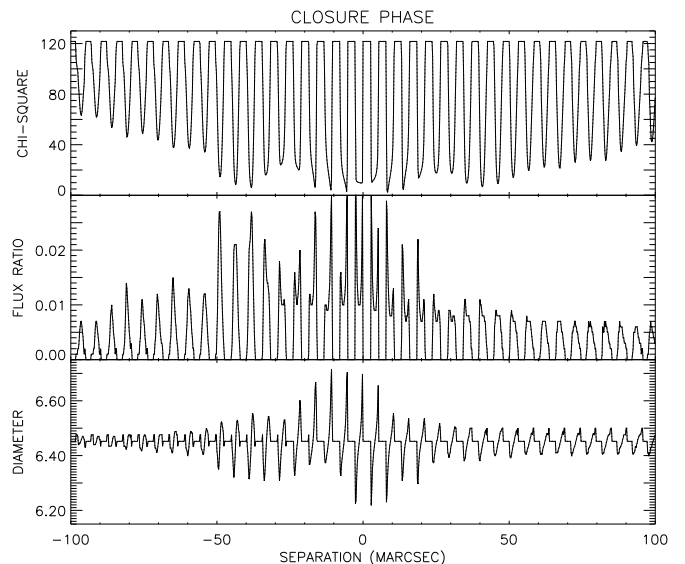


Fig. 5. Best model parameters from the phase closure fit with an extended uniform disk and a point source (see Sect. 3.2 for details). From top to bottom as a function of the separation: minimum χ^2 , best flux ratio and best stellar diameter. The curves represent the best fit with a restricted stellar diameter in the range 6.42–6.48 mas imposed by visibility modelling.

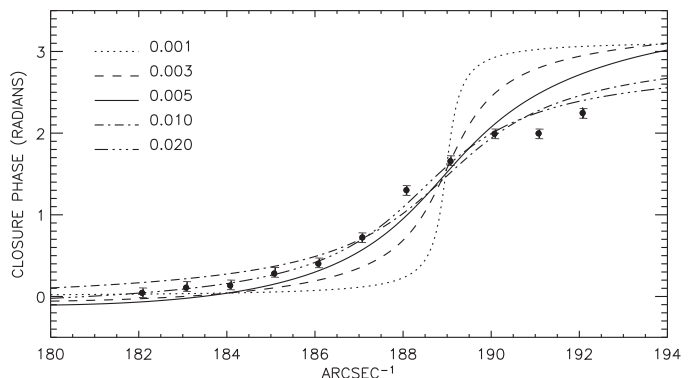


Fig. 6. Best fit of the phase closure for different flux ratios showing that the slope of the transition cannot be reproduced with a flux ratio smaller than 5×10^{-3} .

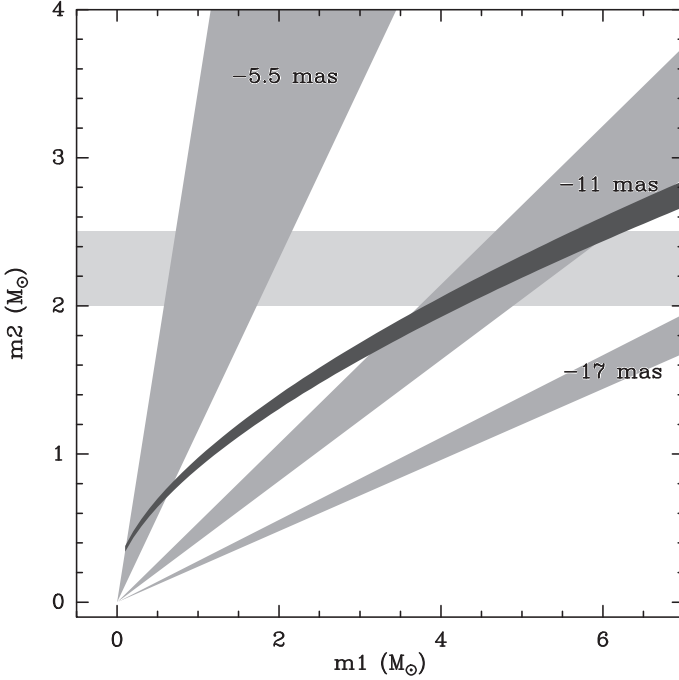
the stellar diameter but support the binary nature of HD 59717 (given the impossibility of reproducing with a single uniform disk model the slope of the phase closure around the minimum of visibility), providing a range of acceptable flux ratios and five possible separations.

4. Discussion

The phase closure transition of HD 59717 is markedly different from that of a single stellar disk. Our modeling of this phase closure transition is naturally based on the *a priori* information that the system is a binary. We do not consider here the influence of large stellar spots because K giants are devoid of such features (Cohen et al. 1999), and because the larger χ^2 of solutions inside the stellar radius in Fig. 5 make it unlikely. Although we detect the faint companion by its effect on the phase closure, the very incomplete information we have on its shape around the first null (compare our Fig. 3 with Fig. 3 of Chelli et al. 2009a) prevents a precise determination of the secondary's position using the in-

Table 2. Literature data for HD 59717 (from Jancart et al. 2005; Wilson 1918; Perryman & ESA 1997).

a_0 (mas)	e	i ($^\circ$)	ω_1 ($^\circ$)	Ω ($^\circ$)	T_0 (JD)	P (d)	dist (pc)	μ (M_\odot)	phot. var. (mmag)
8.32 ± 0.32	0.17	65.6 ± 3.3	349.3	0.0 ± 5.2	2451354.6	257.8	56.36	0.164	30

**Fig. 7.** Loci of the solutions for the equation of mass (black), as a function of the mass m_1 of the primary and m_2 of the secondary. The regions compatible with the set of 3 separations given by our fit are overlaid in gray. The region compatible with our independent measurement of the secondary's flux is overlaid in light gray.

terferometric measurements alone. It is thus important to check whether our results are in agreement with the already known parameters (star diameter, spectroscopic orbit) of HD 59717.

Table 2 summarizes the literature data for HD 59717 relevant to this discussion. HD 59717, at a distance of 56.36 pc, has a spectroscopic period of 257.8 and a reduced mass $\mu = 0.164 M_\odot$ (Wilson 1918). The parameters of the photometric orbit of HD 59717, in particular the inclination $i = 65.6 \pm 3.3$ and semimajor axis $a_0 = 8.32 \pm 0.32$ mas, have been obtained by Jancart et al. (2005) from Hipparcos IAD measurements (van Leeuwen & Evans 1998). HD 59717 exhibits a small amplitude (~ 30 millimag in V) intrinsic variability characteristic of rotating ellipsoidal variables (Perryman & ESA 1997; Otero 2008).

4.1. Stellar diameter of the primary

The stellar diameter of HD 59717 has been estimated by Cohen et al. (1999) who derive a limb-darkened (LD) angular disk diameter of 6.86 ± 0.1 mas. Using the relation between the LD and UD diameters of Hanbury Brown et al. (1974) and a linear limb-darkening coefficient at $2.2 \mu\text{m}$ of 0.379 (Claret et al. 1995), this translates into an equivalent UD diameter in the K band (UDK) of 6.66 ± 0.1 mas. The SearchCal web service (Bonneau et al. 2006) gives $\text{UDK} = 6.16 \pm 0.4$ mas. Our observa-

tions show that the diameter of the primary is well constrained by the visibility data alone to $\text{UDK} = 6.45 \pm 0.03$ mas.

4.2. Nature of the companion

In stellar systems for which all the orbital and projection parameters are measured, the knowledge of the mass m_1 of the main component is sufficient to deduce the mass, hence the spectral type, magnitude, and true orbit of the unseen companion star. Given m_1 , the reduced mass μ , and the inclination i , one solves the equation of mass: $\frac{m_2^3 \sin^3 i}{(m_1 + m_2)^2} = \mu$ for the mass m_2 of the secondary. When the primary is a main-sequence star, m_1 is reliably estimated using a standard mass-luminosity function (e.g., McCluskey & Kondo 1972). Unfortunately, there is no such thing as a unique mass-luminosity function for giant stars (as is the case for HD 59717), so m_1 is unknown and individual masses in a binary system with a giant component cannot be derived reliably by this method.

Conversely, if the *companion* of the giant star is a main-sequence star, and if its luminosity can be measured, then m_2 is known and the mass m_1 of the giant can be measured. In the present case, our observations provide two new pieces of information: the luminosity of the secondary via our measurement of the flux ratio, and a choice of projections of the separation on the E-W direction. Each of these pieces of information can be used independently to derive the mass of the giant primary, and should provide compatible results.

4.2.1. Position constraints

We first combine the constraints due to the measured projected separation and the equation of mass. In Fig. 7 we show the loci of the solutions for the equation of mass with $i = 65.6 \pm 3.3$, $\mu = 0.164 M_\odot$ in black. At the time of our observations, the position angle of the binary was $\theta = -76.0 \pm 1.5$, and the projection of the separation $sp = \alpha(1 + \frac{m_1}{m_2})$, where $\alpha = -3.5 \pm 0.2$ is fixed by the orbit geometry. The positive projected separations (+8.5 and +14 mas) are forbidden by the value of α . The three possible (m_1, m_2) solutions left are for the projected separations -5.5, -11 and -17 mas, and are plotted in Fig. 7 in gray. Their width corresponds to the uncertainty (± 1 mas) on the separation.

The solutions for the binary masses lie at the intersection between these areas and the curve given by the equation of mass. The -5.5 mas and -17 mas regions give unrealistic values for the mass distribution in the binary: the former since the primary would be less massive than the secondary, the latter because it gives a too high mass for the primary. This leaves only the -11 mas solution, and our mass estimate by this method is then a $5 M_\odot$ primary and a $2.2 M_\odot$ secondary.

4.2.2. Photometry constraints

If we use now the magnitude of the secondary derived from our observed flux ratio, its spectral type is A0V–A2V (see Table 3). Then m_2 lies between $2.0 M_\odot$ and $2.5 M_\odot$ (McCluskey & Kondo

Table 3. Known (bold text), measured (italic) and tabulated parameters for the A and B components of the HD 59717 binary.

Star	mK (mag)	MK (mag)	ΔM_k (mag)	MV (mag)	ΔM_v (mag)	Sp.Type	Mass (M_\odot)	Radius (mas) (R_\odot)	$\log g/g_\odot$	$\log \rho/\rho_\odot$	
A	-0.41	-4.16	-	-0.55	-	K5III	5 ± 0.5	3.23 ± 0.015	39	-2.5	-4.7
B	5.14	1.39	5.5	1.8	2.4	A4V	2.0	0.15	1.8	-	-
B	4.89	1.14	5.3	1.3	1.9	A2V	2.2	0.16	2.0	-	-
B	4.59	0.84	5.0	0.65	1.2	A0V	2.5	0.2	2.4	-	-

1972). In Figure 7 we have also reproduced this secondary's mass range as a horizontal area shaded in light gray. It intersects the curve of the equation of mass at $4.5 < m_1 < 5.5 M_\odot$, and thus independently gives the same result as our positional measurement.

Table 3 collects all the parameters on the primary that can be deduced from our size and mass measurements. Three possible identifications are proposed for the B companion, allowing for the uncertainty on the flux ratio. The spectral types and radii of the companion are from Schmidt-Kaler (1982), masses from the mass-luminosity relation of McCluskey & Kondo (1972). We note that the radius and the mass of HD 59717 are larger than the values ($R_{K5III} = 25 R_\odot$ and $M_{K5III} = 1.2 M_\odot$) published by Schmidt-Kaler (1982). However, the masses we obtain are in agreement with the values ($M_{Aa} = 5 M_\odot$, $M_{Ab} > 1.9 M_\odot$) quoted in the MSC catalog (Tokovinin 1997) for the Aab component of HD 59717.

4.3. The photometric variability of HD 59717

The separation of the components, their size, and the inclination of the orbit make it impossible for the secondary to be eclipsed by the primary. With a $5 M_\odot$ primary and a $2.2 M_\odot$ companion, the Roche lobe R_L radius of the primary is $R_L \approx 0.45 \times d$, where d is the true distance of the two stars. Due to the eccentricity $e = 0.17$ of the companion, this distance varies from 23 mas (periastron) to 32 mas (apoastron). With its 3.23 mas radius, the primary thus occupies between 22% and 32% of its Roche lobe, and is slightly ellipsoidal. This is accordance with its classification as a rotating ellipsoidal variable.

If the photosphere of the star was of uniform brightness and shaped by the Roche potential, the maximum prolateness of the star would occur at periastron and be $a/b = 1.0022$. At the time of our observations, the deviation of the projected shape of the star from a circle would be $\sim 6 \times 10^{-4}$, in accordance with our hypothesis that the primary can be modeled as a uniform disk. However, with such a small prolateness, the change in the projected surface of the star with time would be $< 10^{-3}$, which cannot account for the ~ 30 millimag photometric variability, which requires $a/b \sim 1.02$. The variability of HD 59717 could be due to a difference of surface brightness between the hemisphere of the star facing the companion and the other hemisphere. Although this effect should, to a first approximation, translate as a displacement of the photocenter of the star and would not change the phase closure values, it will be investigated more closely in a future study aimed at confirming at another epoch, with dedicated observations, the detection of HD 59717 companion by phase closure nulling.

5. Conclusion

We have shown that, by fitting a simple model on the spectrally-dispersed phase closure measurements made by AMBER on the

bright SB1 binary HD 59717, observed near the first zero of the visibility distribution, we can resolve the close (~ 4 stellar radii at the time of observation) pair with a five magnitude difference in brightness. This result, obtained with only 15 minutes of on-sky integration and 1.8 m apertures, is two magnitudes fainter than reported detection limits (applying Eq. A.2 of Tokovinin et al. 2006, for $\rho = 11$ mas) and is an illustration of the potential of the phase closure nulling method proposed by Chelli et al. (2009a). We have detailed the specific data processing involved, derived the spectral type of the companion and measured the individual masses and sizes of the system (Table 3).

The PCN method employed here is of interest for the characterisation of all faint point-like sources in the immediate vicinity of stars, if the flux from the *primary* is sufficient and with the quite restrictive condition that the primary can be fully resolved by the interferometer. This technique potentially gives access to masses, even spectra, of brown dwarfs and exoplanets (Chelli et al. 2009a). In this paper we have used published astrometric data, since our observations were of incomplete coverage both in spatial frequency and position angle, but dedicated PCN observations taken at different epochs should suffice to characterize companions and fit their orbit. For exoplanets detected by radial velocity techniques, a single PCN measurement of the secondary's position will solve for inclination of the orbit of the planet. Moreover, since radial velocity techniques can be confused by the presence of stellar spots (see Huélamo et al. 2008), PCN can provide the independent detection needed for confirmation of the presence of an exoplanet.

Acknowledgements. We warmly thank H. Beust and X. Delfosse for their help in the arcane fields of stellar photometry and binary orbits. We are greatly indebted to the anonymous referee who made very useful comments on an earlier version of this paper.

This research has made use of the SearchCa1 and ASPRO services of the Jean-Mariotti Centre², of CDS Astronomical Databases SIMBAD and VIZIER, of NASA Astrophysics Data System Abstract Service program.

References

- Beuzit, J.-L., Mouillet, D., Oppenheimer, B. R., & Monnier, J. D. 2007, in *Protostars and Planets V*, ed. B. Reipurth, D. Jewitt, & K. Keil, 717–732
- Bonneau, D., Clausse, J.-M., Delfosse, X., et al. 2006, *A&A*, 456, 789
- Bracewell, R. N. 1978, *Nature*, 274, 780
- Chelli, A., Duvert, G., Malbet, F., & Kern, P. 2009a, *A&A*, 498, 321
- Chelli, A., Hernandez Utrera, O., & Duvert, G. 2009b, *A&A*, submitted
- Claret, A., Diaz-Cordoves, J., & Gimenez, A. 1995, *A&AS*, 114, 247
- Cockell, C. S., Léger, A., Fridlund, M., et al. 2009, *Astrobiology*, 9, 1
- Cohen, M., Walker, R. G., Carter, B., et al. 1999, *AJ*, 117, 1864
- Danchi, W. C., Rajagopal, J., Kuchner, M., Richardson, L. J., & Deming, D. 2006, *ApJ*, 645, 1554
- Gai, M., Menardi, S., Cesare, S., et al. 2004, in *Society of Photo-Optical Instrumentation Engineers (SPIE) Conference Series*, Vol. 5491, Society of Photo-Optical Instrumentation Engineers (SPIE) Conference Series, ed. W. A. Traub, 528

² Available at <http://jmmc.fr>

- Hanbury Brown, R., Davis, J., Lake, R. J. W., & Thompson, R. J. 1974, *MNRAS*, 167, 475
- Huélamo, N., Figueira, P., Bonfils, X., et al. 2008, *A&A*, 489, L9
- Jancart, S., Jorissen, A., Babusiaux, C., & Pourbaix, D. 2005, *A&A*, 442, 365
- Kalas, P., Graham, J. R., Chiang, E., et al. 2008, *Science*, 322, 1345
- Lagrange, A.-M., Gratadour, D., Chauvin, G., et al. 2009, *A&A*, 493, L21
- Lawson, P. R., Lay, O. P., Martin, S. R., et al. 2008, in *Optical and Infrared Interferometry*. Edited by Schöller, M.; Delplancke, F., Danchi, W. C., Vol. SPIE 7013, in press
- Malbet, F., Duvert, G., Kern, P., & Chelli, A. 2008, ATF February 2008 run report, Tech. rep., AMBER Task Force, Doc. No VLT-TRE-AMB-15830-7120 (<http://arxiv.org/abs/0808.1315>)
- Marois, C., Macintosh, B., Barman, T., et al. 2008, *Science*, 322, 1348
- McCluskey, Jr., G. E. & Kondo, Y. 1972, *Ap&SS*, 17, 134
- Otero, S. 2008, *Open European Journal on Variable Stars*, 83, 1
- Perryman, M. A. C. & ESA, eds. 1997, *ESA Special Publication*, Vol. 1200, The HIPPARCOS and TYCHO catalogues. Astrometric and photometric star catalogues derived from the ESA HIPPARCOS Space Astrometry Mission
- Petrov, R. G., Malbet, F., Weigelt, G., et al. 2007, *A&A*, 464, 1
- Schmidt-Kaler, T. 1982, *Landolt-Börnstein - Numerical Data and functional Relationships in Science and Technology, New Series - Group VI Astronomy and Astrophysics*, Vol. 2B, Physical parameters of the stars (Berlin: Springer, 1982)
- Tokovinin, A., Thomas, S., Sterzik, M., & Udry, S. 2006, *A&A*, 450, 681
- Tokovinin, A. A. 1997, *A&AS*, 124, 75
- van Leeuwen, F. & Evans, D. W. 1998, *A&AS*, 130, 157
- Wilson, R. E. 1918, *Lick Observatory Bulletin*, 9, 116
- Woolf, N. & Angel, J. R. 1998, *ARA&A*, 36, 507